Probing vibronic coherence in charge migration in molecules using strong-field sequential double ionization

C. H. Yuen ●* and C. D. Lin ●†

J. R. Macdonald Laboratory, Department of Physics, Kansas State University, Manhattan, Kansas 66506, USA

We propose a scheme for probing vibronic coherence in charge migration in molecules utilizing strong-field sequential double ionization. To demonstrate the feasibility of this approach, we perform full simulations of a pump-probe scheme employing few-cycle intense infrared pulses for N_2 and O_2. We predict that the vibronic coherence between the pumped states will be directly imprinted in experimental observables such as kinetic energy release spectra and branching ratios of the dissociative dications. Our simulations are based on the recently developed density matrix approach for sequential double ionization model [C. H. Yuen and C. D. Lin, Phys. Rev. A **106**, 023120 (2022)], which is capable of efficiently accounting for molecular orientations and enabling direct comparison with experimental results. Our findings strongly encourage the use of this probing scheme in future charge migration experiments.

In a pump-probe experiment for studying molecular dynamics, one strives for a high temporal resolution as well as a large signal-to-noise ratio. While a high temporal resolution can be achieved using isolated attosecond pulses, the photon flux from tabletop light sources is generally too low to be utilized as both the pump and the probe. Higher count rates and larger signal-to-noise ratios can be reached using intense infrared (IR) pulses as the pump or the probe. If the IR pulse is used as the probe, then it is desirable to increase its peak intensity for higher count rates. As the peak intensity increases, the probe laser may cause sequential double ionization (SDI) of the neutral molecule, resulting in molecular fragmentation. Although experimental setups for making intense few-cycle IR laser pulses and coincidence measurement for ion fragments have been widely available [1–7], this probing scheme has been unfavorable due to the lack of theoretical support. Recently, we developed a density matrix approach for sequential double ionization (DM-SDI) of molecules [8,9], which was benchmarked with experiments for N_2 and O_2 at their ground states [1,3]. One of the goals of this Letter is to demonstrate the feasibility of using SDI to probe molecular dynamics.

The dynamics of interest are the charge migration in molecules. Charge migration is typically initiated by the removal of an electron, which leaves the molecular ion in a superposition of electronic states, and then the electron cloud will migrate along the molecular skeleton [10,11]. Probing this process has become increasingly important due to the advancement of attosecond science [12,13], with prospects of observing electron motion in a molecule in real time and ultimately controlling molecular dynamics. A critical problem in charge migration studies is that the nuclear motion will set

in after a few femtoseconds and could lead to the decoherence between different electronic states. Such decoherence would be an obstacle for observing the electron dynamics, but it could lead to a permanent charge transfer to a different site in the molecule, which offers opportunities for controlling its chemical reactivity [14]. While the effects of nuclear motion on charge migration have been studied theoretically [15–19], it remains challenging to monitor the coherence experimentally.

A necessary condition for observing the coherence is that the superposition of states must reach the same final states after the probing process. However, it is not a sufficient condition since the interference signals could be too weak to be observed. This is indeed one of the major challenges in probing the charge migration: It is unclear for what type of molecules and for what type of probing processes such interference signals could be detected. There have been some successful experimental investigations, for example, by using attosecond extreme-ultraviolet (XUV) pump and IR probe [20–22], high-harmonic spectroscopy [23–25], attosecond transient absorption spectroscopy (ATAS) [26–28], attosecond pulse train pump probe [29,30], and femtosecond x-ray pump probe [31,32]. But among these experiments, the types of the target molecules and the probing mechanisms greatly varied, and it is uncertain whether a particular probing scheme will work on other targets. A promising scheme in which the observables could be fully simulated is the ATAS [33,34], but the interference signals may vanish after averaging over molecular orientations due to the anisotropy of the coherence. The search for a general and experimentally accessible probing scheme for charge migration in molecules is therefore of great importance.

SDI could be an excellent process for probing coherence in charge migration since it is driven by laser couplings between the ionic states [8,9]. Suppose a pump laser singly ionizes the neutral molecule and forms a superposition of ionic states.
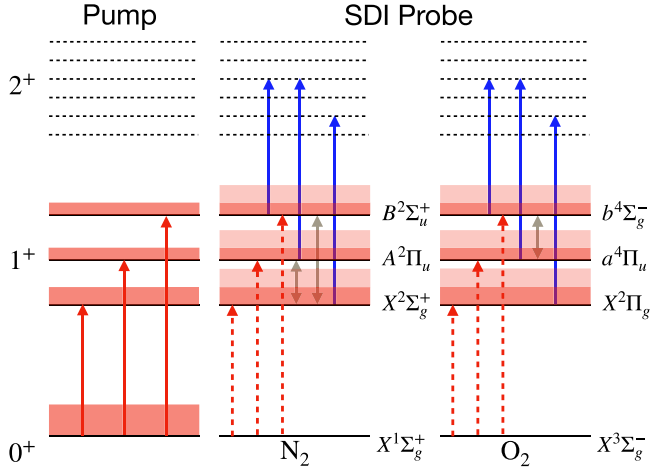
*iyuen@phys.ksu.edu

†cdlin@phys.ksu.edu

FIG. 1. Illustration of the charge migration pump-probe scheme for N_2 and O_2. The pump laser populates the lowest three ionic states (red solid arrows) and the populations are represented by the shaded areas. At a later time, the intense few-cycle IR probe pulse ionizes the remaining neutral population (red dashed arrows), couples the ionic states (gray solid arrows), and tunnel ionizes them to form dications (blue solid arrows). The coherence between the pumped states influences the dication yield through interference with the nascent ionic states (lightly shaded areas) and the laser couplings.

Then, the IR probe will create nascent ionic states, couple the ionic states, and further ionize them to dications. The coherence between the pumped states controls the transient ionic populations through interference with the nascent ionic states and the laser couplings. Since the dication yields depend on the transient ionic populations, the yields will change with the coherence as well. As a result, the coherence could be revealed in experimental observables such as kinetic energy release (KER) spectra or branching ratios of the dications, which always survive the orientation averaging. Figure 1 illustrates this pump-probe scheme for N_2 and O_2. Since the mechanism of SDI should be general for any molecules and the required experimental setups are widely available, the SDI process can serve as a general probing scheme for charge migration. We note that the SDI probe could be similar to the IR probe used in Refs. [21,22], where some dication yields were measured.

In this Letter, we provide compelling evidence of the viability of using the SDI process to probe charge migration in molecules. This is supported by complete simulations on the pump-probe scheme in Fig. 1 for N_2 and O_2 using the DM-SDI model [8,9], which takes molecular orientations into full account such that the results can be directly compared with future experiments. We discover that the vibronic coherence between the pumped states is remarkably imprinted in the KER spectra and branching ratios for $N^+ + N^+$ and $O^+ + O^+$ at different pump-probe delays. The findings of this Letter strongly encourage future experiments to use the SDI probe for charge migration in N_2 and O_2 as well as other molecules.

The DM-SDI model is based on a density matrix approach and can describe the evolution of population and coherence of different charge states due to laser couplings and tunneling ionization simultaneously [8,9]. To make the model simple, we assume that the nuclei of the molecule are frozen in the

presence of a few-cycle IR pulse and neglect the ionized electrons such that different charge states are incoherent. Since many-body electronic wave functions are not explicitly involved and the nuclei are frozen, the computational cost of the model is low and one can compare the calculated results under experimental conditions by averaging over the molecular orientations and the focal volume. The predictive power of the model has been well demonstrated recently in Refs. [8,9] by reproducing the main features of the KER spectra in SDI experiments of N_2 and O_2 [1,3]. For details of the model, we refer the reader to our previous articles [8,9]. Briefly, the equations of motion for the density matrices $\rho^{(q)}$ are

$$\frac{d}{dt}\rho^{(q)}(t) = -\frac{i}{\hbar}[H^{(q)}(t), \rho^{(q)}(t)] + \Gamma^{(q)}(t), \quad (1)$$

where $q = 0, 1, 2$ is the charge of the molecule and $H^{(q)}(t) = H_0^{(q)} - \vec{d} \cdot \vec{E}(t)$, with $H_0^{(q)}$ being the field-free Hamiltonian, $\vec{d}$ being the dipole moment, and $\vec{E}$ being the electric field. The ionization rate matrices $\Gamma^{(0)}(t) = -\sum_i \rho^{(0)}(t) W_i^{(0)}(t)$ and $\Gamma_{mn}^{(2)}(t) = \delta_{mn} \sum_i \rho_{ii}^{(1)}(t) W_{n\leftarrow i}^{(1)}(t)$ describes the depopulation of the only neutral state and the population of the nth state of the dication, where $W_i^{(0)}$ and $W_{n\leftarrow i}^{(1)}$ are the molecular Ammosov-Delone-Krainov ionization rates [35] from the neutral to the ith ionic state and from the ith ionic state to the nth state of the dication, respectively. As the ionic states interact via laser couplings, coherence builds up between them. To account for the dephasing of the ions from the tunnel ionization to dications, we extend our previous model [8,9] for the ion as

$$\Gamma_{ij}^{(1)}(t) = \delta_{ij}\rho^{(0)}(t)W_i^{(0)}(t)$$

$$- \rho_{ij}^{(1)}(t)\sqrt{\sum_n W_{n\leftarrow i}^{(1)}(t)}\sqrt{\sum_n W_{n\leftarrow j}^{(1)}(t)}. \quad (2)$$

The modeling of the dephasing term is because $|\rho_{ij}^{(1)}| \propto \sqrt{\rho_{ii}^{(1)}\rho_{jj}^{(1)}}$ and $d\rho_{ii}^{(1)}/dt \sim -\rho_{ii}^{(1)}\sum_n W_{n\leftarrow i}^{(1)}$, such that $\rho_{ij}^{(1)}$ should decay with the population.

The simulation for the pump-probe scheme consists of these three steps: the pump, the free propagation, and the probe. For simplicity in both theory and experiment, we consider the pump and probe pulse to be a few-cycle IR pulse.

(i) For the pumping process, we solved Eq. (1) at the equilibrium geometry of the neutral molecule for a 6 fs, 800 nm, linearly polarized Gaussian pulse with a peak intensity of 3×10^{14} W/cm^2 for each angle θ between the laser polarization and the molecular axis. The initial conditions are set as $\rho^{(0)}(\theta, t_0) = 1$ and $\rho^{(1)}(\theta, t_0) = \rho^{(2)}(\theta, t_0) = 0$, such that there is only neutral population before the pump pulse. Then, the highest occupied molecular orbital (HOMO), HOMO-1, and HOMO-2 of the molecule are ionized to form a superposition of ionic states (cf. Fig. 1), and at the end of the pump laser ($t = t_1$), density matrices $\rho^{(0)}(\theta, t_1)$ and $\rho^{(1)}(\theta, t_1)$ are obtained. Since the peak intensity is weak, the dication yield from the pumping process is negligible such that $\rho^{(2)}(\theta, t_1) = 0$. We set $t = 0$ at the peak of the pump pulse and $t_1 = 6$ fs.

(ii) For the free propagation, we assume that after the pump pulse, the vibrational states of the ion are populated according to their Franck-Condon (FC) factors. The nuclear wave function of the ith ionic state $|\chi_i(t)\rangle$ then evolves as
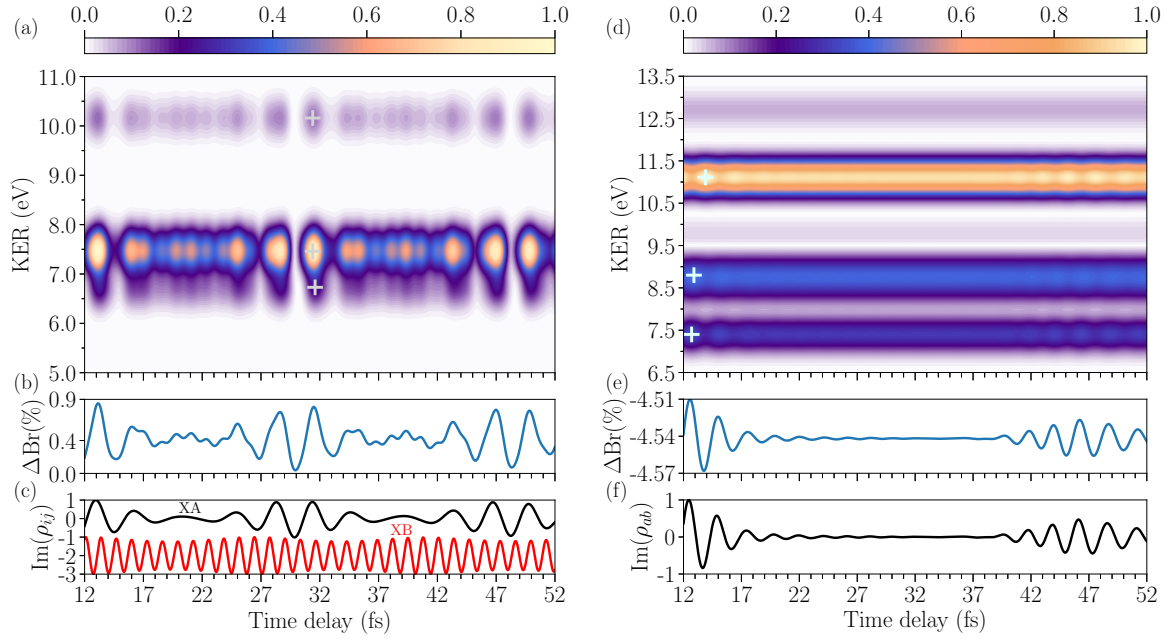
FIG. 2. (a),(d) Simulated KER spectra for (a) $N^+ + N^+$ and (d) $O^+ + O^+$ as a function of pump-probe delays, subtracted by the respective probe-only signal. The markers show the phase differences of the beating between different KER peaks. Note that in (d) the spectra are more negative with higher values. (b),(e) Branching ratio of $N^+ + N^+$ and $O^+ + O^+$ over their respective total dication yield as a function of pump-probe delay, subtracted by the probe-only ratio. (c) Imaginary part of the off-diagonal density matrix elements between the $X\,^2\Sigma_g^+$ and $A\,^2\Pi_u$ states (black) and the $X\,^2\Sigma_g^+$ and $B\,^2\Sigma_u^+$ states (red) of N_2^+ at $\theta = 45°$. The red curve is shifted down for better visualization. (f) Same as (c), but for the $a^4\Pi_u$ and $b^4\Sigma_g^-$ states of O_2^+. Due to the interference of formation pathways of the dications, the time dependence of the density matrix elements in (c) and (f), which represent the vibronic coherence between the ionic states, are reflected in (a),(b) and (d),(e), respectively.

$|\chi_i(t)\rangle = \sum_v |c_{iv}||\phi_{iv}\rangle e^{-iE_{iv}t}$, where $|c_{iv}|^2$ is the FC factor from the neutral vibronic ground state to the v level of the ith ionic state, $|\phi_{iv}\rangle$ is the vibrational wave function, and E_{iv} is the vibronic energy. To simulate the change in coherence due to the nuclear motion of the ion during the pump-probe delay, within the FC approximation, we model the vibronic coherence $\rho_{ij}^{(1)}(\theta, t)$ for $t > t_1$ as [16]

$$\rho_{ij}^{(1)}(\theta, t) = C_{ij}(\theta)\langle\chi_j(t - t_1)|\chi_i(t - t_1)\rangle, \qquad (3)$$

where $C_{ij}(\theta)$ is a constant to match the matrix element at $t = t_1$. Note that the nuclear overlap function $\langle\chi_j|\chi_i\rangle$ is independent of θ since the nuclear motion occurs in the molecular frame and is irrespective of the molecular orientations. Details about the nuclear overlap functions can be found in Sec. S1 of the Supplemental Material (SM) [36].

(iii) For the probing process, we consider the probe pulse to be the same as the pump, but with a peak intensity of 1.2×10^{15} W/cm^2. To account for the vibronic coherence at a later time t, we solved Eq. (1) again for each θ, but with the initial conditions $\rho^{(0)}(\theta, t) = \rho^{(0)}(\theta, t_1)$, $\rho^{(1)}(\theta, t)$ as in Eq. (3), and $\rho^{(2)}(\theta, t) = 0$. The validity of using Eqs. (1) and (3) for the probing process is proved by a rigorous derivation using the fixed nuclei and FC approximation (see Sec. S2 of the SM [36]). Finally, after the probe pulse, we average the yield of each dication state over θ, assign the KER peak for each state, and convolve the peaks with experimental energy resolution to simulate the KER spectra, as was done in Refs. [8,9]. Note that

we neglect the focal volume effect since it does not change the qualitative behavior of the KER spectra [8,9].

The main results of this Letter are shown in Fig. 2. The time delay τ, which is defined as the time difference between the peak of the two laser pulses with the pump pulse arriving first, begins at 12 fs in order to minimize the overlap of the pulses. Figures 2(a) and 2(d) show the simulated KER spectra for $N^+ + N^+$ and $O^+ + O^+$ as a function of time delay, subtracted by the respective probe-only signal. One can see clear beatings at the highest peak of the spectra for both N_2 (7.5 eV) and O_2 (11 eV). The beating for N_2 weakens starting from $\tau = 15$ fs (corresponding to 3 fs after the pump pulse), but revives shortly at $\tau = 28$ fs, and similar patterns occur from $\tau = 31$ to 47 fs. Meanwhile, the beating for O_2 dampens from $\tau = 15$ fs and almost vanishes during $\tau = 19$ to 39 fs. At $\tau > 40$ fs, one can see the revival of the beating.

The weakening and revival of the beatings in Figs. 2(a) and 2(d) are due to the change of vibronic coherence at different time delays. If we neglect the vibrational motion during the pump-probe delays, the beatings for both N_2 and O_2 would simply repeat the pattern from $\tau = 12$ to 14 fs due to the infinitely long-lived coherence (see Sec. S3 of the SM [36]). Note that the weaker peaks for N_2 and O_2 beat similarly as the main peaks, but some with phase shifts [see the markers in Figs. 2(a) and 2(d)]. These phase shifts are due to different formation pathways to the dication states. A detailed discussion can be found in Sec. S3 of the SM [36].

To further understand the link between the vibronic coherence and the KER spectra, we compare the branching ratios
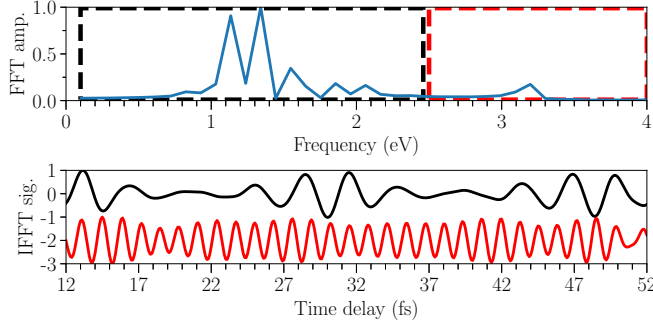
FIG. 3. Top: Fast Fourier transform (FFT) spectra of Fig. 2(b) for N_2^+. To retrieve the vibronic coherence between the $X\,^2\Sigma_g^+$–$A\,^2\Pi_u$ and the $X\,^2\Sigma_g^+$–$B\,^2\Sigma_u^+$ states of N_2^+, inverse FFT (IFFT) was performed on the signal inside the black and red boxes (and the negative counterparts). Bottom: Respective IFFT signals, with the red curve being shifted down for better visualization.

for dissociative dications in Figs. 2(b) and 2(e) with the off-diagonal density matrix elements of the ion in Figs. 2(c) and 2(f) at different time delays. The plotted branching ratios are the total yield of dissociative dications over the total yield of dications at a time delay τ, subtracted by the probe-only ratio. Off-diagonal elements $\rho_{ij}(\tau)$ at $\theta = 45°$ are plotted as an example. One can see that the branching ratios are closely related to the imaginary part of ρ_{ij} for both N_2^+ and O_2^+. Such a relationship results from the equation of motion for the population of the ion [derived from Eq. (1) for a fixed θ],

$$\frac{d}{dt}\rho_{ii}^{(1)}(t) = -2\sum_l \vec{d}_{il} \cdot \vec{E}(t)\,\mathrm{Im}\left[\rho_{li}^{(1)}(t)\right] + \Gamma_{ii}^{(1)}(t). \quad (4)$$

From the first term on the right, one can see that the vibronic coherence $\rho_{li}^{(1)}$ regulates the population transfer between ionic states through the laser couplings. Since the dication yields depend on the transient ionic populations $\rho_{ii}^{(1)}$, the dication yields also depend on the vibronic coherence.

The relationship between the branching ratio and the vibronic coherence is target dependent and state dependent. In the case of N_2^+, as there are two pairs of laser-coupled states, its branching ratio is beating at two different sets of vibronic frequencies [see Fig. 2(b)]. Since the $X\,^2\Sigma_g^+$–$A\,^2\Pi_u$ beating (taken as 1.35 eV) is near resonant with the 800 nm laser (1.55 eV) while the $X\,^2\Sigma_g^+$–$B\,^2\Sigma_u^+$ beating (3.17 eV) is off resonant, the branching ratio mostly depends on the $X\,^2\Sigma_g^+$–$A\,^2\Pi_u$ coherence. Note that the $X\,^2\Sigma_g^+$–$B\,^2\Sigma_u^+$ coherence is long lived. For O_2^+, since only the $a\,^4\Pi_u$ and $b\,^4\Sigma_g^-$ states are coupled by the laser, their vibronic coherence is directly imprinted to the branching ratio [see Fig. 2(e)].

An important consequence of this work is that one can directly retrieve the vibronic coherence from experiments. Since the nuclear overlap functions are independent of molecular orientation, the retrieval makes sense even if the molecules are not aligned. The top panel of Fig. 3 shows the fast Fourier transform (FFT) spectra of Fig. 2(b) for N_2^+. There are two sets of beatings: one for $X\,^2\Sigma_g^+$–$A\,^2\Pi_u$ (black box) and one for $X\,^2\Sigma_g^+$–$B\,^2\Sigma_u^+$ (red box). The $X\,^2\Sigma_g^+$–$A\,^2\Pi_u$ vibronic beatings could be four times stronger than the $X\,^2\Sigma_g^+$–$B\,^2\Sigma_u^+$ beating, as expected from the near-resonant condition. One can perform an inverse FFT (IFFT) for the spectra in the black and red boxes (and the same range in negative frequencies) to retrieve the vibronic coherence for the two pairs of states. The bottom panel of Fig. 3 shows the retrieved IFFT signals for N_2^+, and one can see that both signals are in good agreement with the vibronic coherence in Fig. 2(c). Similar analysis can be done for O_2^+, but because only the $a\,^4\Pi_u$ and $b\,^4\Sigma_g^-$ states are coupled by the laser, the IFFT spectra will simply reproduce Fig. 2(e).

In summary, we have shown that it is feasible to use the SDI as a probe for molecular dynamics. While the vibronic coherence in charge migration in molecules is known to be challenging to probe, we showed that the SDI probe offers a simple and viable solution since it is driven by laser couplings between ionic states, and is thereby sensitive to their coherence. Such conclusions can be drawn from our simulations because our model takes into account experimental conditions, such as isotropic distribution of molecular orientations, which are rarely addressed by other theoretical studies based on first-principles approaches.

The essence of our theoretical approach is in the separation of the treatment of the laser-molecule interaction and the nuclear dynamics. Because of the use of few-cycle IR pulses, the former can be dealt with using the DM-SDI model [8,9] at fixed nuclei, while the latter can be modeled by field-free quantum chemistry approaches in the molecular frame [15,17]. Therefore, the computational cost of the simulation is significantly reduced and the orientation averaging can be performed to directly compare the results with experiments. Consequently, the current approach could be extended to more complex molecules.

With the recent advancement of pulse compression techniques, it is now possible to generate few-cycle to even single-cycle IR pulses [37]. This theoretical and experimental progress will open up numerous research opportunities for probing molecular dynamics utilizing the SDI process and the ultrashort pulses.

[1] S. Voss, A. S. Alnaser, X. M. Tong, C. Maharjan, P. Ranitovic, B. Ulrich, B. Shan, Z. Chang, C. D. Lin, and C. L. Cocke, J. Phys. B: At. Mol. Opt. Phys. **37**, 4239 (2004).

[2] A. S. Alnaser, S. Voss, X.-M. Tong, C. M. Maharjan, P. Ranitovic, B. Ulrich, T. Osipov, B. Shan, Z. Chang, and C. L. Cocke, Phys. Rev. Lett. **93**, 113003 (2004).

[3] Z. Wu, C. Wu, X. Liu, Y. Liu, Y. Deng, and Q. Gong, Opt. Express **18**, 10395 (2010).

[4] S. De, I. A. Bocharova, M. Magrakvelidze, D. Ray, W. Cao, B. Bergues, U. Thumm, M. F. Kling, I. V. Litvinyuk, and C. L. Cocke, Phys. Rev. A **82**, 013408 (2010).

[5] S. De, M. Magrakvelidze, I. A. Bocharova, D. Ray, W. Cao, I. Znakovskaya, H. Li, Z. Wang, G. Laurent, U. Thumm, M. F. Kling, I. V. Litvinyuk, I. Ben-Itzhak, and C. L. Cocke, Phys. Rev. A **84**, 043410 (2011).

[6] X. Xie, K. Doblhoff-Dier, H. Xu, S. Roither, M. S. Schöffler, D. Kartashov, S. Erattupuzha, T. Rathje, G. G. Paulus, K. Yamanouchi, A. Baltuska, S. Grafe, and M. Kitzler, Phys. Rev. Lett. **112**, 163003 (2014).

[7] C. Cheng, Z. L. Streeter, A. J. Howard, M. Spanner, R. R. Lucchese, C. W. McCurdy, T. Weinacht, P. H. Bucksbaum, and R. Forbes, Phys. Rev. A **104**, 023108 (2021).

[8] C. H. Yuen and C. D. Lin, Phys. Rev. A **106**, 023120 (2022).

[9] C. H. Yuen, P. Modak, Y. Song, S.-F. Zhao, and C. D. Lin, Phys. Rev. A **107**, 013112 (2023).

[10] L. S. Cederbaum and J. Zobeley, Chem. Phys. Lett. **307**, 205 (1999).

[11] A. S. Folorunso, A. Bruner, F. Mauger, K. A. Hamer, S. Hernandez, R. R. Jones, L. F. DiMauro, M. B. Gaarde, K. J. Schafer, and K. Lopata, Phys. Rev. Lett. **126**, 133002 (2021).

[12] F. Krausz and M. Ivanov, Rev. Mod. Phys. **81**, 163 (2009).

[13] J. Biegert, F. Calegari, N. Dudovich, F. Quéré, and M. Vrakking, J. Phys. B: At., Mol. Opt. Phys. **54**, 070201 (2021).

[14] F. Lépine, M. Y. Ivanov, and M. J. Vrakking, Nat. Photon. **8**, 195 (2014).

[15] V. Despré, A. Marciniak, V. Loriot, M. Galbraith, A. Rouzée, M. Vrakking, F. Lépine, and A. Kuleff, J. Phys. Chem. Lett. **6**, 426 (2015).

[16] C. Arnold, O. Vendrell, and R. Santra, Phys. Rev. A **95**, 033425 (2017).

[17] N. V. Golubev, T. Begušić, and J. Vaníček, Phys. Rev. Lett. **125**, 083001 (2020).

[18] D. Dey, A. I. Kuleff, and G. A. Worth, Phys. Rev. Lett. **129**, 173203 (2022).

[19] A. Scheidegger, J. Vaníček, and N. V. Golubev, J. Chem. Phys. **156**, 034104 (2022).

[20] G. Sansone, F. Kelkensberg, J. Pérez-Torres, F. Morales, M. F. Kling, W. Siu, O. Ghafur, P. Johnsson, M. Swoboda, E. Benedetti *et al.*, Nature (London) **465**, 763 (2010).

[21] F. Calegari, D. Ayuso, A. Trabattoni, L. Belshaw, S. De Camillis, S. Anumula, F. Frassetto, L. Poletto, A. Palacios, P.

Decleva, J. B. Greenwood, F. Martin, and M. Nisoli, Science **346**, 336 (2014).

[22] M. Lara-Astiaso, M. Galli, A. Trabattoni, A. Palacios, D. Ayuso, F. Frassetto, L. Poletto, S. De Camillis, J. Greenwood, P. Decleva, I. Tavernelli, F. Calegari, M. Nisoli, and F. Martin, J. Phys. Chem. Lett. **9**, 4570 (2018).

[23] O. Smirnova, Y. Mairesse, S. Patchkovskii, N. Dudovich, D. Villeneuve, P. Corkum, and M. Y. Ivanov, Nature (London) **460**, 972 (2009).

[24] P. M. Kraus, B. Mignolet, D. Baykusheva, A. Rupenyan, L. Horný, E. F. Penka, G. Grassi, O. I. Tolstikhin, J. Schneider, F. Jensen *et al.*, Science **350**, 790 (2015).

[25] L. He, S. Sun, P. Lan, Y. He, B. Wang, P. Wang, X. Zhu, L. Li, W. Cao, P. Lu, and C. D. Lin, Nat. Commun. **13**, 1 (2022).

[26] Y. Kobayashi, K. F. Chang, S. M. Poullain, V. Scutelnic, T. Zeng, D. M. Neumark, and S. R. Leone, Phys. Rev. A **101**, 063414 (2020).

[27] Y. Kobayashi, D. M. Neumark, and S. R. Leone, Phys. Rev. A **102**, 051102(R) (2020).

[28] D. T. Matselyukh, V. Despré, N. V. Golubev, A. I. Kuleff, and H. J. Wörner, Nat. Phys. **18**, 1206 (2022).

[29] T. Okino, Y. Furukawa, Y. Nabekawa, S. Miyabe, A. Amani Eilanlou, E. J. Takahashi, K. Yamanouchi, and K. Midorikawa, Sci. Adv. **1**, e1500356 (2015).

[30] S. Fukahori, T. Matsubara, Y. Nabekawa, K. Yamanouchi, and K. Midorikawa, J. Phys. B: At., Mol. Opt. Phys. **53**, 164001 (2020).

[31] T. Barillot, O. Alexander, B. Cooper, T. Driver, D. Garratt, S. Li, A. Al Haddad, A. Sanchez-Gonzalez, M. Agåker, C. Arrell *et al.*, Phys. Rev. X **11**, 031048 (2021).

[32] D. Schwickert, M. Ruberti, P. Kolorenč, S. Usenko, A. Przystawik, K. Baev, I. Baev, M. Braune, L. Bocklage, M. K. Czwalinna *et al.*, Sci. Adv. **8**, eabn6848 (2022).

[33] R. Santra, V. S. Yakovlev, T. Pfeifer, and Z.-H. Loh, Phys. Rev. A **83**, 033405 (2011).

[34] N. V. Golubev, J. Vaníček, and A. I. Kuleff, Phys. Rev. Lett. **127**, 123001 (2021).

[35] X.-M. Tong, Z. X. Zhao, and C.-D. Lin, Phys. Rev. A **66**, 033402 (2002).

[36] See Supplemental Material at http://link.aps.org/supplemental/10.1103/PhysRevA.109.L011101 for details about the nuclear overlap functions, derivation of the equations of motion for the density matrices, and additional details about the KER spectra.

[37] M.-S. Tsai, A.-Y. Liang, C.-L. Tsai, P.-W. Lai, M.-W. Lin, and M.-C. Chen, Sci. Adv. **8**, eabo1945 (2022).